MCB
Journals.ASM.org

Cernunnos Deficiency Reduces Thymocyte Life Span and Alters the T Cell Repertoire in Mice and Humans

Gabriella Vera,[a,b] Paola Rivera-Munoz,[a,b] Vincent Abramowski,[a] Laurent Malivert,[a,b] Annick Lim,[d] Christine Bole-Feysot,[b] Christelle Martin,[e] Benoit Florkin,[f] Sylvain Latour,[a,b] Patrick Revy,[a,b] Jean-Pierre de Villartay[a,b,c]

Laboratory of Genome Dynamics in the Immune System, INSERM U768, Paris, France[a]; Université Paris Descartes-Sorbonne Paris Cité, Institut Imagine, Site Necker, IFR94, Paris, France[b]; Assistance Publique-Hôpitaux de Paris, Service d'Immunologie et d'Hématologie Pédiatrique, Hôpital Necker Enfants Malades, Paris, France[c]; Département d'Immunologie, Institut Pasteur, Paris, France[d]; SEAT, CNRS UPS44, Villejuif, France[e]; Service de Pédiatrie, Centre Hospitalier Universitaire de la Citadelle, Liège, Belgium[f]

Cernunnos is a DNA repair factor of the nonhomologous end-joining machinery. Its deficiency in humans causes radiosensitive severe combined immune deficiency (SCID) with microcephaly, characterized in part by a profound lymphopenia. In contrast to the human condition, the immune system of Cernunnos knockout (KO) mice is not overwhelmingly affected. In particular, Cernunnos is dispensable during V(D)J recombination in lymphoid cells. Nevertheless, the viability of thymocytes is reduced in Cernunnos KO mice, owing to the chronic activation of a P53-dependent DNA damage response. This translates into a qualitative alteration of the T cell repertoire to one in which the most distal Vα and Jα segments are missing. This results in the contraction of discrete T cell populations, such as invariant natural killer T (iNKT) and mucosa-associated invariant T (MAIT) cells, in both humans and mice.

The immune system is the site of intense genome dynamics, in particular during the development and maturation of B and T lymphocytes in bone marrow and the thymus, when antigen receptor genes are rearranged through V(D)J recombination prior to their expression. DNA damages are also likely to occur during the several phases of intense proliferation which accompany the development of B and T cells.

V(D)J recombination is the prototypical example of the generation of a programmed DNA double-strand break (DNA-dsb) during lymphoid development through the activity of recombination activating genes 1 and 2 (Rag1/2) on immunoglobulin (Ig) and T cell receptor (TCR) genes (see the work of Helmink and Sleckman [1] for a recent review). The resulting DNA-dsb is resolved by the nonhomologous end-joining (NHEJ) DNA repair pathway, composed of seven core components (see the work of Lieber [2] for a recent review). The Cernunnos-Xrcc4-DNA ligase IV complex ultimately reseals the DNA-dsb. Cernunnos, also known as Xrcc4-like factor (XLF), was the last NHEJ factor that was independently identified, through a survey of RS-SCID patients (3) and a yeast two-hybrid screen with Xrcc4 as a bait (4). Cernunnos and Xrcc4 adopt the same overall three-dimensional crystal structure (5, 6) and, together with DNA ligase IV, are parts of the same complex (4, 7). Cernunnos stimulates the DNA-joining activity of the Xrcc4-DNA ligase IV complex (8, 9).

V(D)J recombination constitutes a central checkpoint in the development of the immune system, as its defect leads to abortive B and T cell maturation *in vivo*, resulting in severe combined immune deficiency (SCID) (10), but its first recognized function was the generation of a diverse antigenic repertoire through the combinatorial association of variable, diversity, and joining segments that encode the variable domains of both Ig and TCRs (11). Numerous examples show that a reduced V(D)J recombinase activity affects the extent of antigenic diversity of immune receptors in mice and humans. The resulting immune deregulation may then lead to autoimmunity, increased susceptibility to infections, or the development of various forms of cancer (12).

A Cernunnos knockout (Cernu KO) mouse in which deletion of exons 4 and 5 caused in-frame alternative splicing of exon 3 to 6 and residual (<1% of wild-type [wt] level) protein expression was previously reported (13). In the present study, we used a different gene targeting approach to develop a complete Cernunnos null mouse model to explore the role of Cernunnos in the development and maturation of the murine immune system in comparison to what is known of Cernunnos-deficient human patients.

MATERIALS AND METHODS

Generation of Cernu$^{-/-}$ mice. Cernu$^{-/-}$ mice were developed at the Institut Clinique de la Souris (ICS; Illkirch, France) by flanking exon 4 with LoxP sites (Fig. 1). Mice were genotyped by standard PCR on tail DNA by use of the following primers: Cernu4R (5′-GTCCCCAGCTGTT AAGAGTTTC-3′) for KO and flox mice, CernuExo4F (5′-GGATGAAG GACCTTGAGATCC-3′) for flox mice, and Cernu3F (5′-CTATGGAAG CCAGGAGAGAATG-3′) for KO mice. All animals were maintained in a specific-pathogen-free environment. Analyses were performed on Cernu KO and littermate control animals on a mixed B6/129 background. P53 KO mice were on a mixed B6/129 background as well. All experiments and procedures were performed in compliance with the French Ministry of Agriculture's regulations for animal experiments (act 87847, 19 October 1987; modified in May 2001).

Analysis of lymphocyte populations. Cell phenotyping was performed on blood, thymus, bone marrow, lymph nodes, and splenic lymphoid populations by four-color fluorescence analysis as previously described (14).

Invariant natural killer T cell (iNKT cell) determination was performed on splenocytes from 4- to 8-week-old mice by staining with allophycocyanin (APC)–mouse CD1d tetramer, loaded or not loaded with

Received 2 August 2012 Returned for modification 28 September 2012
Accepted 26 November 2012
Published ahead of print 3 December 2012
Address correspondence to Jean-Pierre de Villartay, devillartay@gmail.com.
G.V., P.R.-M., and V.A. contributed equally to this article.

doi:10.1128/MCB.01057-12

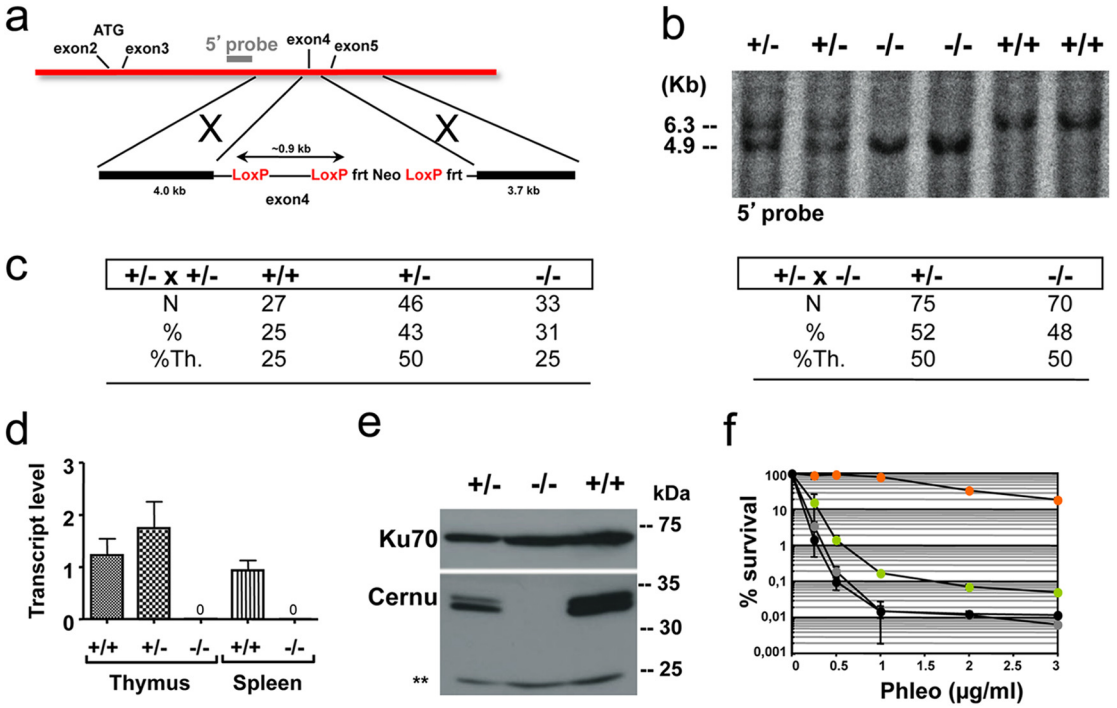

FIG 1 Generation of Cernu$^{-/-}$ mice. (a) Schematic representation of the KO strategy and location of the external 5′ probe. Exon 4 was flanked by LoxP sites. (b) Southern blot analysis of tail DNA by use of a 5′ probe. The blot shows the 6.3-kb wt band and the 4.9-kb KO allele on a BclI digest. (c) Mendelian distributions of genotypes in offspring of Cernu$^{+/-}$ × Cernu$^{+/-}$ and Cernu$^{+/-}$ × Cernu$^{-/-}$ intercrosses. %Th., percent theoretical. (d) Quantitative RT-PCR evaluation of Cernunnos transcript levels in thymuses and spleens of +/+, +/−, and −/− littermates. (e) Western blot analysis showing the absence of the 35-kDa Cernunnos protein in MEFs. Anti-Ku-70 antibody was used as a loading control. **, nonspecific band. (f) Phleomycin sensitivity of Cernu$^{-/-}$ (green circles), Xrcc4$^{-/-}$ (gray circles), DNA Lig4$^{-/-}$ (black circles), and wt (orange circles) MEFs. The data represent one of two separate experiments, with values representing the means of two independent determinations for each point.

αGal-cer (kindly provided by the NIH Tetramer Core Facility); 2.4G2 anti-Fc antibody and fluorescein isothiocyanate (FITC)–anti-mouse TCR-β (both from BD Bioscience); and phycoerythrin (PE)–anti-mouse CD3ε and anti-mouse NK1.1 (both from Becton Dickinson). Human iNKT cells (15) and mucosa-associated invariant T cells (MAIT cells) (16) were detected using anti-Va24 and anti-Va7.2 antibodies on peripheral blood lymphocytes (PBLs).

V(D)J recombination assay in thymocytes. CD4$^-$ CD8$^-$ thymocytes were negatively purified by magnetic sorting and infected with MX-RSS12/23 supernatant (17). The level of V(D)J recombination was determined 48 h after transduction by scoring the GFP$^+$ (rearranged) cells among the human CD4-positive (huCD4$^+$) transduced cells. Thymocytes from Artemis$^{-/-}$ mice were used as a negative control.

Thymocyte proliferation assay *in vivo*. Cernu KO mice were bred into the Rag1$^{-/-}$ background, and 6- to 8-week-old double-KO (DKO) mice were injected intraperitoneally (i.p.) with 100 μg of anti-CD3 antibody to mimic the TCR-β selection-induced thymocyte proliferative burst as previously described (18).

Thymocyte survival assay *in vitro*. Single-cell suspensions were obtained from the thymus and cultured at 1×10^6 cells/ml in Dulbecco's modified Eagle's medium (DMEM) supplemented with glutamine and 10% decomplemented fetal bovine serum. The number of viable cells after 24 h was counted by trypan blue staining, and apoptosis was analyzed by fluorescence-activated cell sorting (FACS) after labeling with annexin V and 7-aminoactinomycin D (7AAD) (apoptosis detection kit; BD Pharmingen).

Reverse transcription-PCR (RT-PCR) analysis of TCR Jα usage. For combined determinations of mTRAV3.1, mTRAV5.1, and mTRAV3.4 usage, thymocyte- and splenocyte-derived cDNAs were PCR amplified using mTRAV3 (5′-TCATCTGCACCTACACAGACAGTGC-3′) and mTCR-EX4R (5′-GATGGAGCTTGGGAGTCAG-3′) primers, cloned into the TOPO-TA vector (Invitrogen), and sequenced with T7 or M13 primers. Immunoscope analysis was performed as previously described (19).

Analysis of global TCR-α usage by deep sequencing. RNAs from human PBLs were reverse transcribed using a Smarter 5′ rapid amplification of cDNA ends (5′RACE) kit (Clontech Laboratories) according to the manufacturer's recommendations. 5′RACE PCR was achieved using a mix of long (5′-CTAATACGACTCACTATAGGGCAAGCAGTGGTATCAACGCAGAGT-3′) and short (5′-CTAATACGACTCACTATAGGGC-3′) primers in a universal primer mix (UPM), along with the Cα reverse primer CAR3 (5′-GTCTCTCAGCTGGTACACG-3′). Five-hundred-base-pair PCR products were gel purified and processed for single-molecule sequencing using an Ion personal genome machine (PGM) (Ion Torrent, Life Technologies) according to the manufacturer's recommendations. hTRAV and hTRAJ gene segments were identified using the IMGT database and software (http://www.imgt.org/HighV-QUEST) (20). The genomic location of each hTRAV and hTRAJ element was obtained from the UCSC Genome Browser (http://genome.ucsc.edu/).

Quantitative real-time RT-PCR analysis. TaqMan PCR was performed on triplicates of 20 ng of reverse-transcribed RNA, using predesigned primer and probe sets from Applied Biosystems (for mouse Cernunnos exons 1 and 2, set Mm 01259071_m1; for mouse Bid exons 5 and 6, set Mm 00432073_m1; for mouse Cdkn1a or P21 exons 1 and 2, set Mm 01303209_m1; for mouse Bax exons 4 and 5, set Mm 00432050 _m1; for mouse Bbc3 or PUMA exons 3 and 4, set Mm 00519268 _m1; and for glyceraldehyde-3-phosphate dehydrogenase [GAPDH], set Mm 99999915_g1). mRNA content was calculated with SDS2.1 sequence detector software (Applied Biosystems). GAPDH was used for normalization of expression, and

a

	Thymus		Spleen		LN	
	+/-	-/-	+/-	-/-	+/-	-/-
Cells (x10°)+/- SEM	108.7+/-14.3 (n=20)	31.6+/-8.4 (n=10)	72.8+/-8.0 (n=17)	27.4+/-2.8 (n=12)	6.7+/-1.1 (n=10)	4.7+/-1.2 (n=6)
	p=0.0009		p<0.0001		p=0.25	

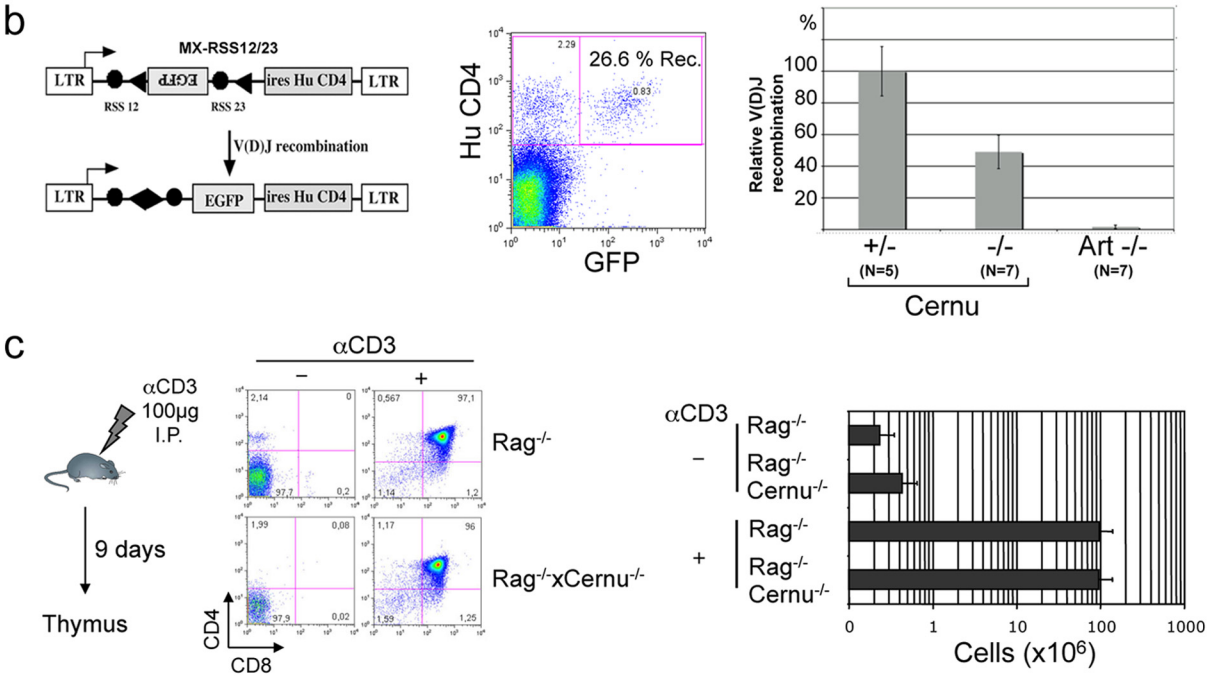

FIG 2 (a) Lymphocyte cellularity in thymuses, spleens, and lymph nodes (LN) of Cernu$^{+/-}$ and Cernu$^{-/-}$ mice. SEM, standard error of the mean. (b) V(D)J recombination activity in purified CD4$^-$ CD8$^-$ thymocytes. Transduced cells were identified through expression of the huCD4 gene from the reporter. The % recombination represents the fraction of GFP-positive cells among the huCD4-positive cells. The relative V(D)J activity was calculated by comparison to the level attained in thymocytes from Cernu$^{+/-}$ mice, used as a 100% activity control. (c) Proliferative capacity of thymocytes. Cernu$^{-/-}$ Rag1$^{-/-}$ and Rag1$^{-/-}$ mice were injected i.p. with anti-CD3.

RNA from Cernu$^{+/-}$ mice was used as the calibrator. The relative amounts of mRNA in samples were determined using the $2^{-\Delta\Delta CT}$ method, where $\Delta\Delta C_T$ is the difference between ΔC_T($C_T$target − C_TGAPDH) sample and ΔC_T($C_T$target − C_TGAPDH) calibrator. Final results are expressed as *n*-fold differences in target gene expression for tested samples compared with the mean expression value for the control.

RESULTS

Generation of Cernunnos KO mice. Based on previous structure-function studies, we designed our Cernunnos KO model by deleting exon 4 (Fig. 1a). Cernu KO mice were bred to homozygosity by crossing of Cernu$^{+/-}$ mice. All genotype combinations were observed at the expected Mendelian frequencies (Fig. 1b and c). Quantitative RT-PCR analysis covering exons 1 and 2 demonstrated the absence of detectable Cernunnos transcripts in both thymuses and spleens from Cernu$^{-/-}$ mice as a probable consequence of nonsense-mediated RNA decay resulting from the out-of-frame splicing of exons 3 to 5 (Fig. 1d). Accordingly, Cernunnos protein was not detected in Cernu$^{-/-}$ murine embryonic fibroblasts (MEFs) by Western blotting (Fig. 1e). MEFs from Cernu$^{-/-}$ mice demonstrated an increased sensitivity to the radiomimetic drug phleomycin *in vitro* (Fig. 1f), as expected for an NHEJ defect.

The immune system is not overwhelmingly affected in Cernunnos KO mice. The lymphocyte counts of Cernu$^{-/-}$ mice were slightly yet significantly diminished (Fig. 2a) compared to those of their wt littermates in the thymus (31.6×10^6 versus 108.7×10^6; $P = 0.0009$), spleen (27.4×10^6 versus 72.8×10^6; $P < 0.0001$), and lymph nodes (6.7×10^6 versus 4.7×10^6; $P = 0.25$), in contrast with the known severe lymphopenia of human Cernunnos patients (3). This was independent of the age of the animals (data not shown) and homogeneous between all T and B cell populations analyzed for the thymus, spleen, and lymph nodes (data not shown). The lark-shaped image of CD4/CD8 dual staining of thymocytes attests the normal development of thymocytes through all maturation stages and thus indicates a proficient V(D)J recombination process. To confirm this, we analyzed the V(D)J recombination activity *ex vivo* in purified DN thymocytes, using the retroviral V(D)J recombination substrate MX-RSS12/23 (17) (Fig. 2b). About 26% of thymocytes from wt mice transduced with the reporter (identified by the expression of huCD4) had rearranged the substrate and expressed green fluorescent protein (GFP). No recombination could be identified in Artemis-deficient thymocytes, as expected. DN thymocytes from Cernu$^{-/-}$ mice showed a 2-fold reduction in V(D)J recombination activity in this setting. Moreover, sequences of coding joints recovered from Cernu$^{-/-}$ thymocytes were only marginally affected, with a slight yet not statistically significant increase in coding end erosion com-

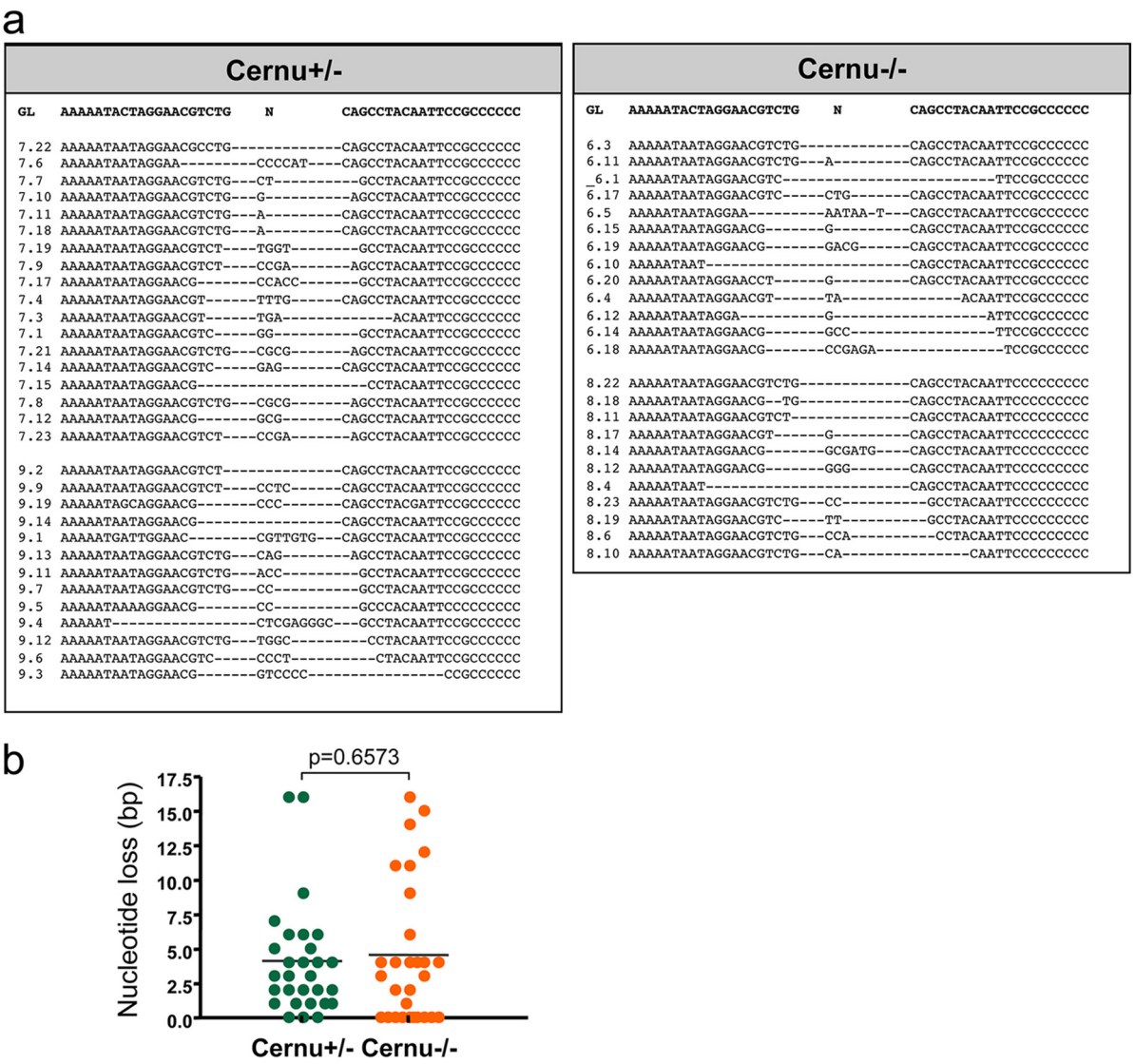

FIG 3 (a) Nucleotide sequence analysis of coding joints recovered from pMX-RSS-12/23-transduced thymocytes from 2 Cernu$^{+/-}$ and 2 Cernu$^{-/-}$ mice. (b) Similar frequencies of nucleotide loss at coding joints recovered from pMX-RSS-12/23-transduced thymocytes from Cernu$^{+/-}$ and Cernu$^{-/-}$ mice.

pared with that in wt thymocytes (Fig. 3). This is in accord with the relatively normal V(D)J recombination activity noted in Abelson murine leukemia virus (A-MuLV)-transformed pro-B cell lines derived from a distinct Cernu$^{-/-}$ mouse model (13). Cernunnos is also dispensable for V(D)J recombination in humans, as shown by normal B cell differentiation in the bone marrow in Cernunnos-deficient patients as opposed to Rag1/2-, Artemis-, or DNA ligase IV-deficient patients (21).

We then asked if the reduction in thymocyte counts could be a consequence of an impaired proliferative capacity during TCR-β selection. We introduced the Cernu KO mutation on the Rag1$^{-/-}$ background and mimicked the TCR-β selection-driven thymocyte proliferative burst by treating mice i.p. with 100 μg anti-CD3 as previously described (18). There was no difference in anti-CD3-driven thymocyte expansion after 9 days between Rag1$^{-/-}$ × Cernu$^{-/-}$ and Rag1$^{-/-}$ mice, with about 100 × 10^6 recovered cells, a 2-log increase compared to the thymocyte cellularity of untreated mice in both cases (Fig. 2c).

The T cell repertoire is biased in Cernunnos KO mice. We analyzed the T cell repertoire diversity in Cernu$^{-/-}$ mice by immunoscope analysis (19). Both TCR-β (Fig. 4a) and TCR-α (Fig. 4b) repertoires were diversified, with the representation of all Vβ and Vα families in accord with the proficient V(D)J recombination activity. Nevertheless, a close examination of the most 5′ (distal) and 3′ (proximal) Vα segments revealed a striking difference in their usage among Cernu$^{-/-}$ and Cernu$^{+/-}$ mice (Fig. 4b and c). Whereas the distal mTRAV1 and mTRAV2 segments accounted for 2.2% of all Vα segments in Cernu$^{+/-}$ T cells, they represented only 0.4% of Vα segments in Cernu$^{-/-}$ mice (Fig. 4c). Conversely, the most proximal segments, i.e., mTRAV17 to mTRAV21, represented 2.7% and 8.8% of Vα segments in Cernu$^{+/-}$ and Cernu$^{-/-}$ T lymphocytes, respectively. In other words, while the frequency of distal Vα segments was reduced by 80% in Cernu$^{-/-}$ T cells, the usage of proximal Vα segments was increased 3.2-fold in the same mice. To consolidate this observation, we designed a PCR assay whereby TCR-α transcripts ex-

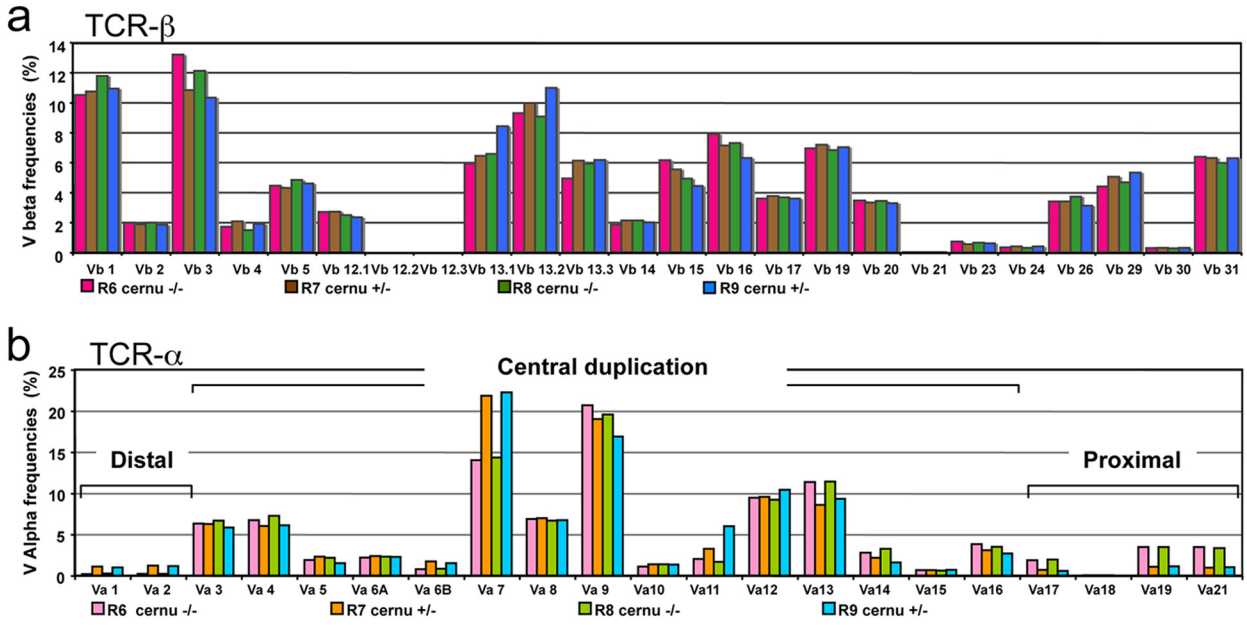

c

	Vα dist. (Va1,Va2)	Vα prox. (Va17-Va21)
Cernu$^{+/-}$	2.29% 2.15%	2.73% 2.73%
Cernu$^{-/-}$	0.40% 0.47% ↘ x 0.2	8.88% 8.80% ↗ x 3.2

FIG 4 Immunoscope analysis of TCR-β (a) and TCR-α (b) repertoires from 2 Cernu$^{-/-}$ (R6 and R8) and 2 Cernu$^{+/-}$ (R7 and R9) mice. (c) Differential representation of distal (5′) and proximal (3′) Vα segments in Cernu$^{-/-}$ and Cernu$^{+/-}$ T cells.

pressing either distal mTRAV3.1 and mTRAV5.1 genes or the proximal mTRAV3.4 gene (Fig. 5a) are coamplified with a single pair of primers and the frequencies of the three Vα segments then determined by cloning and sequencing. As shown in Fig. 5b, the use of distal Vα segments was significantly reduced in Cernu$^{-/-}$ mice compared to Cernu$^{+/-}$ mice, in both the thymus (32% versus 81%; $P < 0.0001$) and the spleen (61% versus 81%; $P < 0.0001$). We next determined the Jα usage of each set of distal and proximal Vα-containing TCR-α transcripts (Fig. 5c). In accordance with the theory of sequential waves of TCR-α rearrangements in the thymus (see Discussion) (22), the proximal Vα (Vα3′)-containing transcripts tended to use the most 5′ (proximal to Vαs) Jα segments, with medians at mTRAJ51 in the thymus and mTRAJ46 in the spleen for both Cernu$^{+/-}$ and Cernu$^{-/-}$ T cells. The distal Vα (Vα5′)-containing transcripts from Cernu$^{+/-}$ T cells followed the same rule by using more 3′ (distal to Vαs) Jα segments centered around mTRAJ16 and mTRAJ25 in the thymus and the spleen, respectively. In sharp contrast, distal Vα-containing transcripts from Cernu$^{-/-}$ T cells contained Jα segments centered on mTRAJ40 and mTRAJ46 in the thymus and the spleen, respectively, close to the beginning of the TCR Jα cluster. In summary, the molecular analysis of TCR-α rearrangements in Cernu$^{-/-}$ mice revealed two main differences compared to Cernu$^{+/-}$ mice: (i) a strong tendency to use the most 3′ (proximal to Jαs) Vα segments and (ii) a considerable shift in Jα usage toward the most 5′ (proximal to Vαs) segments even when TCR-α rearrangements involved distal Vαs.

The TCR-α repertoire is skewed in human Cernunnos patients. We then wished to appreciate to what extent the variation of Vα and Jα utilization identified in Cernu$^{-/-}$ mice could be generalized to the human Cernunnos deficiency condition. We evaluated the TCR-α repertoire in PBLs by means of 5′RACE PCR and next-generation sequencing (NGS). Vα and Jα sequences were plotted according to their relative positions in the genome (Fig. 6a and b). Whereas the median position of Vα in TCR-α transcripts from a control individual was located around hTRAV9.2 (at bp 3.2×10^5), the median Vα position in TCR-α transcripts from a Cernunnos patient was significantly displaced downstream of the Vα locus, around hTRAV26-1 (at bp 5.2×10^5), in proximity to the TCR Jα cluster. Conversely, the median Jα segments were centered around hTRAJ28 and hTRAJ39 (at bp 4.0×10^4 and 2.6×10^4) in the control and the Cernunnos patient, respectively, with a statistically significant shift toward the 5′ side of the TCR Jα cluster, more proximal to the Vα segments, in the TCR-α repertoire from the patient. A contour plot representation of the TCR-α transcripts according to the positions of Vα and Jα segments (Fig. 6b) illustrates the shift of the TCR-α point cloud toward the most downstream Vα and most upstream Jα segment in PBLs from the Cernunnos patient compared to the control. Indeed, the barycenter (Vα; Jα) moved from (bp 3.2×10^5; bp $4.0 \times$

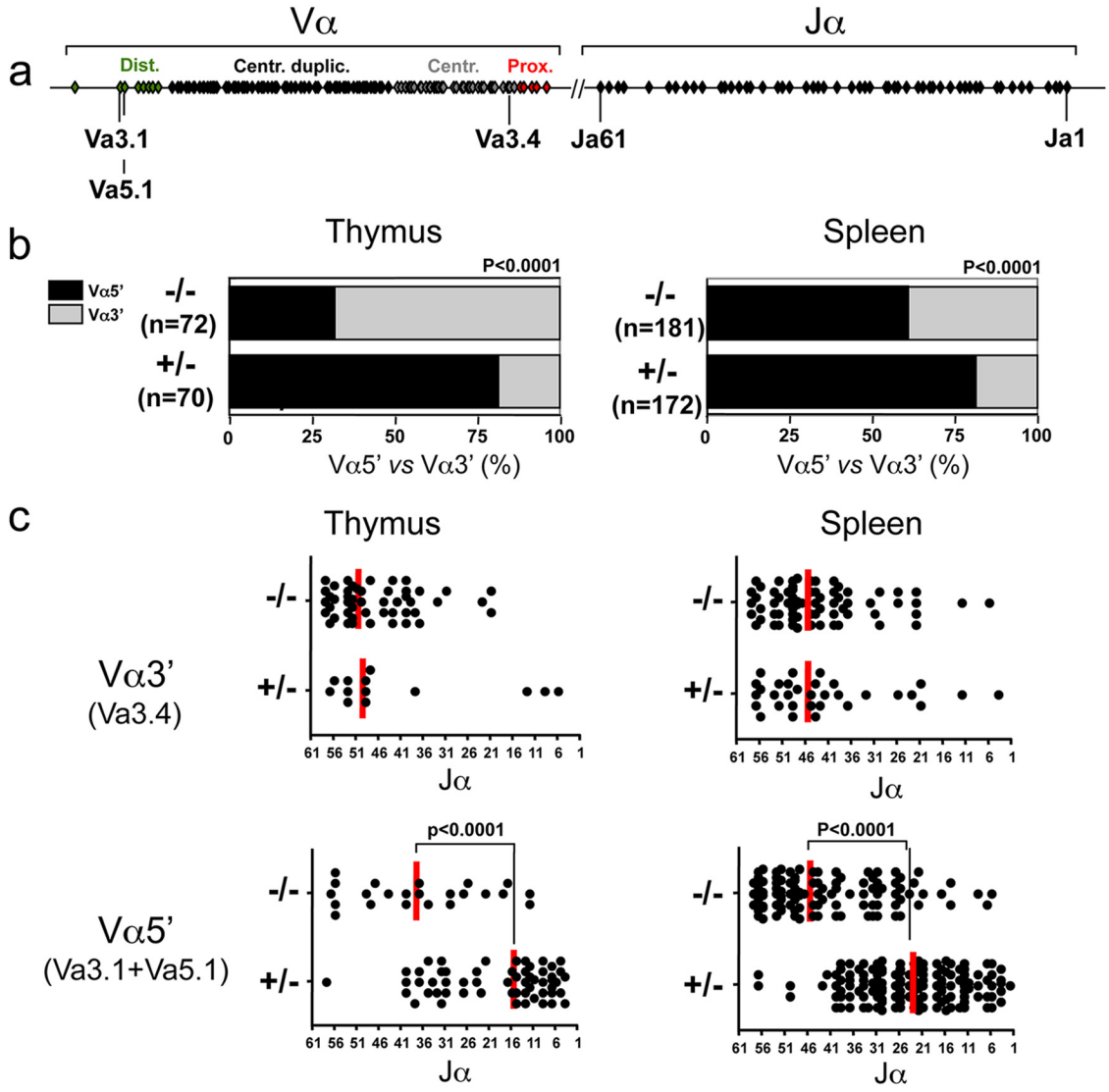

FIG 5 (a) Schematic representation of murine TCR Vα and Jα clusters and positions of the three Vα genes coamplified by PCR using a unique set of primers. (b) Differential representation of distal Vαs (mTRAV3.1 and mTRAV5.1) versus proximal Vαs (mTRAV3.4) after cloning and sequencing of RT-PCR products from the thymus and the spleen. (c) TCR Jα representation in distal and proximal Vα-containing transcripts from thymuses and spleens of Cernu$^{-/-}$ and Cernu$^{+/-}$ mice. Vertical red lines correspond to the medians for Jα usage.

10^4) in the control to (bp 5.2×10^5; bp 2.6×10^4) in the Cernunnos patient.

MAIT and iNKT cells are two innate-like populations of T lymphocytes that express highly conserved and semi-invariant T cell receptors (23, 24). iNKT cells are bona fide T lymphocytes that also express NK lineage receptors. They recognize microbial ligands, suggesting their probable innate-like antimicrobial functions. MAIT cells also react to bacterially infected cells, in a major histocompatibility complex (MHC) class I-like molecule (MR1)-dependent manner. Vitamin B metabolites were recently identified as ligands for MAIT cells (25). In humans, iNKT cells use hTRAV10 (at bp 2.0×10^5) and hTRAJ18 (at bp 5.0×10^4), and MAIT cells express hTRAV1.2 (at bp 0.2×10^5) and hTRAJ33 (at bp 3.3×10^4). Figure 6c represents the positions of invariant TCR-α transcripts from iNKT and MAIT cells together with the 75% cloud points of TCR-α transcripts from a Cernunnos patient and a control individual. It appears that MAIT and iNKT cell-specific TCR-α transcripts are well outside the TCR-α 75% cloud point for the Cernunnos patient, arguing that these two minor T cell populations should largely be underrepresented in the context of Cernunnos deficiency. In mice, the invariant TCR-α repertoire expressed by iNKT cells is composed of Vα14 (mTRAV11) rearranged to mTRAJ18. The frequency of iNKT cells identified by dual staining using anti-TCR-β and a CD1d tetramer decreased significantly, from 1.06% to 0.28%, in the spleens of Cernu$^{-/-}$ mice (Fig. 7b), as expected given the reduced usage of distal TCR Jα segments. Determination of the numbers of iNKT and MAIT cells in PBLs from one Cernunnos patient showed the same tendency, with a 10-fold decrease in both populations in comparison with the control for the day (data not shown). Nevertheless, since the frequencies of iNKT and MAIT cells are highly variable among individuals, this sole observation in humans awaits other cases for statistical support.

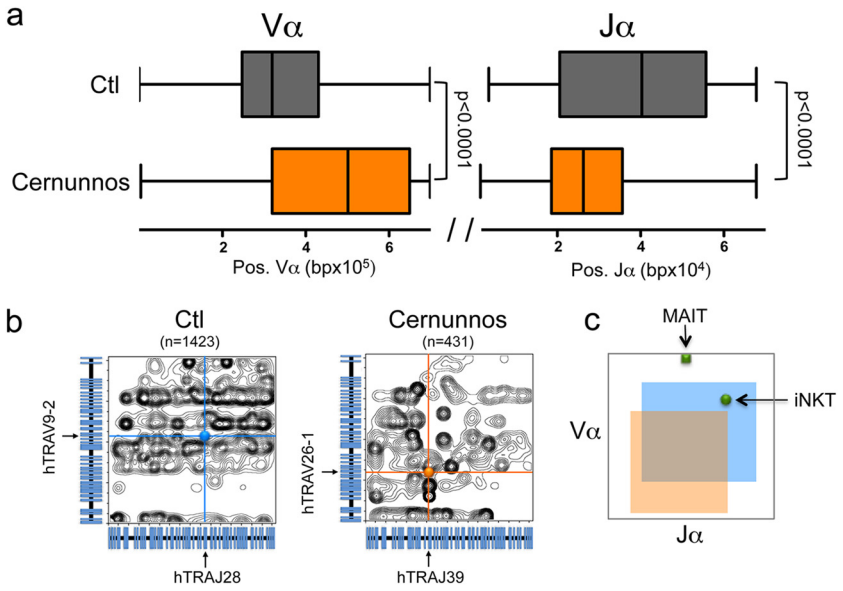

FIG 6 TCR-α repertoire in a human Cernunnos patient. (a) Box-and-whisker representation of Vα and Jα usage in TCR-α transcripts from one Cernunnos patient and one control individual as determined by 5′RACE PCR and NGS. Each VαJα transcript (orange and gray areas for the Cernunnos patient and the control individual, respectively) is positioned according to the relative locations (in bp) of its Vα and Jα elements in the genome. (b) Contour plot representation of TCR-α transcripts from a Cernunnos patient (431 sequences) and a control individual (1,423 sequences). Blue and orange bullets represent the VαJα barycenter in each case. (c) Boxes representing 75% of TCR-α transcript sequences for a Cernunnos patient (orange square) and a control individual (blue square). The two green bullets represent the theoretical positions of TCR-α chains from iNKT (hTRAV10, at bp 2.0×10^5; and hTRAJ18, at bp 5.0×10^4) and MAIT (hTRAV1.2, at bp 0.2×10^5; and hTRAJ33, at bp 3.3×10^4) cells, respectively.

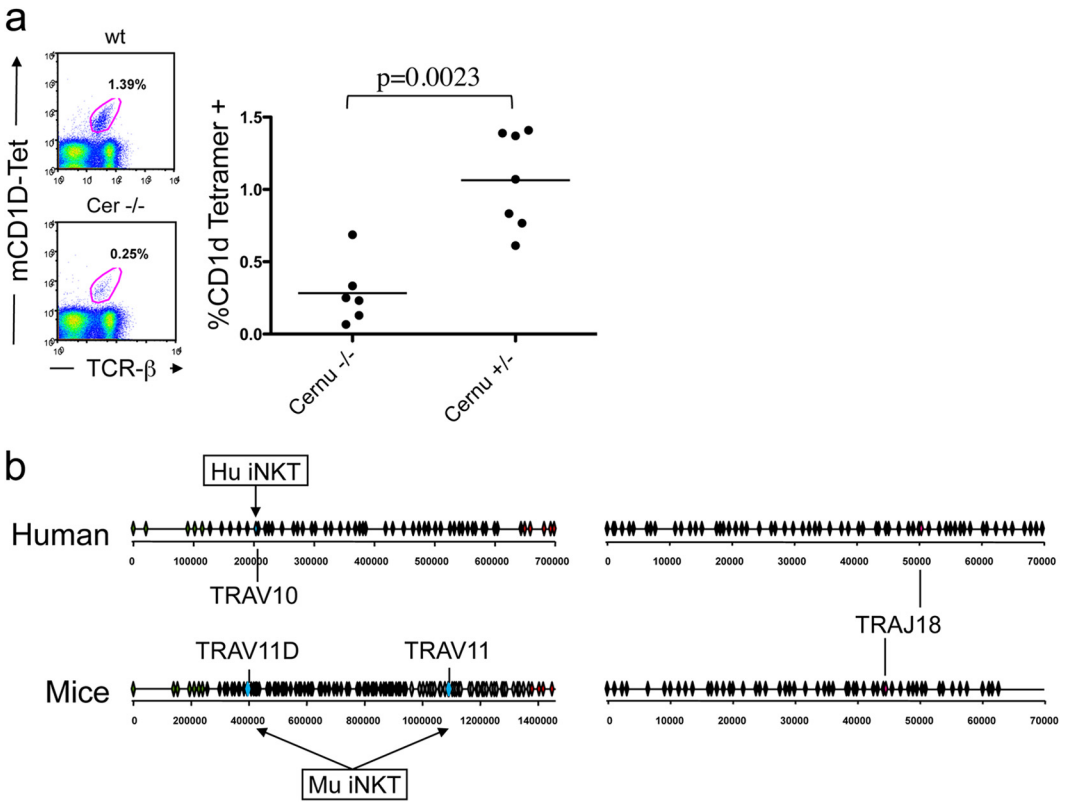

FIG 7 (a) Detection of iNKT cells in the spleen by dual staining with anti-TCR-β and CD1d tetramer. (b) Schematic representation of human and murine TCR Vα and Jα clusters, including the locations of TRAV and TRAJ used by iNKT cells. Two Jα segments can be used by murine NKT cells, i.e., TRAV11D and the most downstream segment, TRAV11, because of the duplication of the central TCR Jα segments in mice.

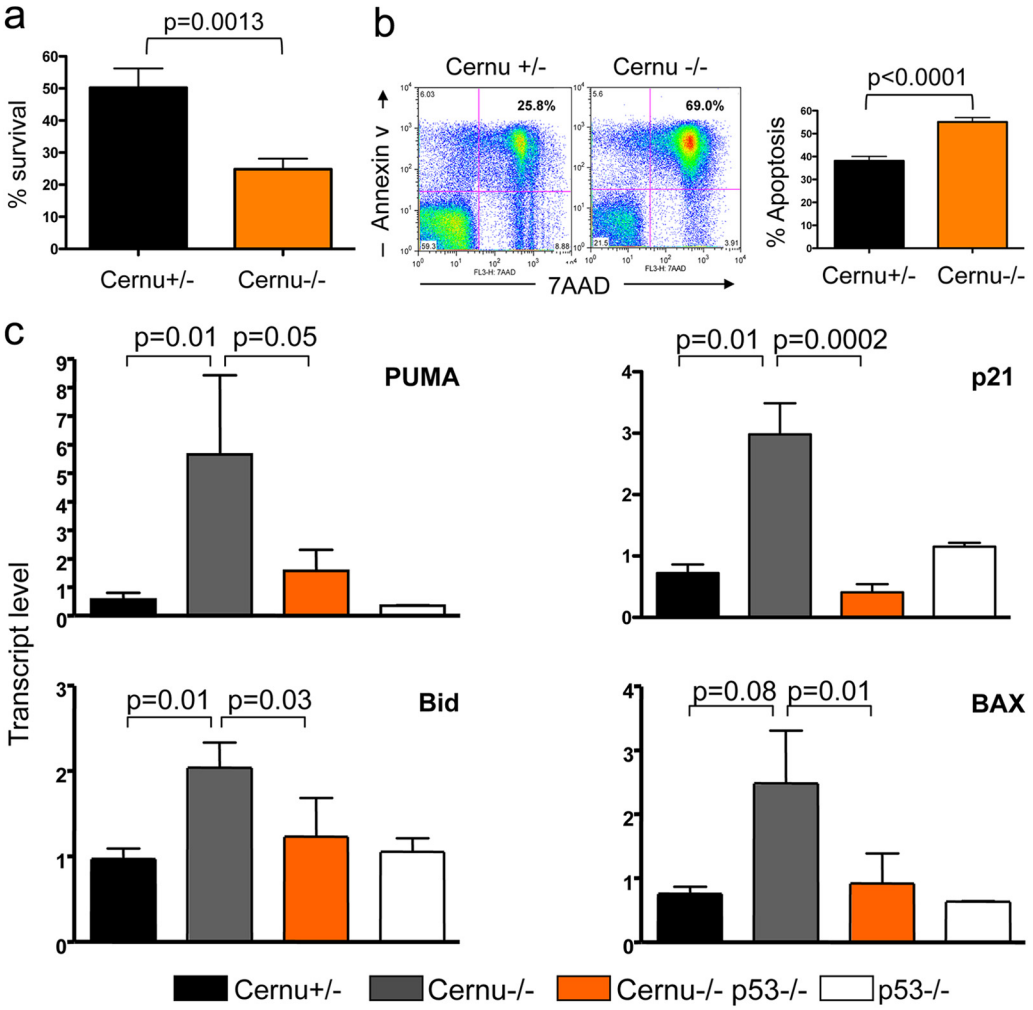

FIG 8 Thymocyte survival (a) and apoptosis (b) in 24-h cultures *in vitro*. (c) Quantitative RT-PCR analysis of P53 target genes in Cernu$^{-/-}$ thymocytes.

Collectively, the shift in TCR-α usage toward the most proximal Vα and Jα segments and the resulting disappearance of iNKT cells represent the signature of reduced thymocyte viability as detailed in Discussion. This series of analyses thus suggested that the lack of Cernunnos decreases the thymocyte life span in both humans and mice.

Decreased viability of Cernu$^{-/-}$ thymocytes. To confirm this hypothesis, we analyzed the thymocyte life span upon Cernunnos inactivation by surveying thymocyte viability after 24 h in culture *in vitro* (Fig. 8a). The cell recovery decreased from 50.22% to 24.84% in Cernu$^{+/-}$ and Cernu$^{-/-}$ cultures, respectively. This statistically significant 50% reduction was imputable to an increase in thymocyte apoptosis as measured by dual staining with 7AAD and annexin V (Fig. 8b).

To evaluate the possible implication of the DNA repair/tumor suppressor factor P53 in this phenomenon, we determined the levels of expression of several P53 target genes by real-time quantitative PCR (Fig. 8c). The expression of four P53-dependent genes involved in apoptosis, i.e., PUMA, P21, Bid, and BAX, was significantly increased in thymocytes from Cernu$^{-/-}$ mice (Fig. 8c). The almost complete return of expression levels to baseline for these four genes in the Cernu$^{-/-}$ × P53$^{-/-}$ DKO animals further supported the implication of P53 in thymocyte apoptosis caused by the loss of Cernunnos.

P53 KO partly complements reduced Cernunnos KO thymocyte viability. To further ascertain the role of P53 in the decreased thymocyte fitness observed in Cernu$^{-/-}$ mice, we generated Cernu$^{-/-}$ × P53$^{-/-}$ DKO animals and surveyed the various parameters associated with thymocyte viability. The first striking consequence of introducing the P53 KO background was a complete normalization of the thymocyte counts (243.2×10^6 in DKO mice versus 92.78×10^6 in Cernu$^{-/-}$ mice; $P = 0.0074$) in DKO mice (Fig. 9a), together with a statistically significant increase in thymocyte recovery in 24-h *in vitro* cultures (Fig. 9b). Introduction of the P53 KO background also had a significant impact on the frequencies of TCR Vα and Jα usage (Fig. 9c). Indeed, the proportion of upstream Vα usage increased from 32% to 58% in splenic T cells from Cernu$^{-/-}$ and DKO mice, respectively, with a statistically significant shift toward the values obtained for T cells from wt (93%) and P53$^{-/-}$ (82%) mice. This partial normalization of TCR Vα usage was accompanied by a concomitant correction of Jα usage in Vα5′-containing transcripts, with median Jα positions at mTRAJ38 and mTRAJ29 in Cernu$^{-/-}$ and DKO T cells, respectively, with the mTRAJ position in the latter approach-

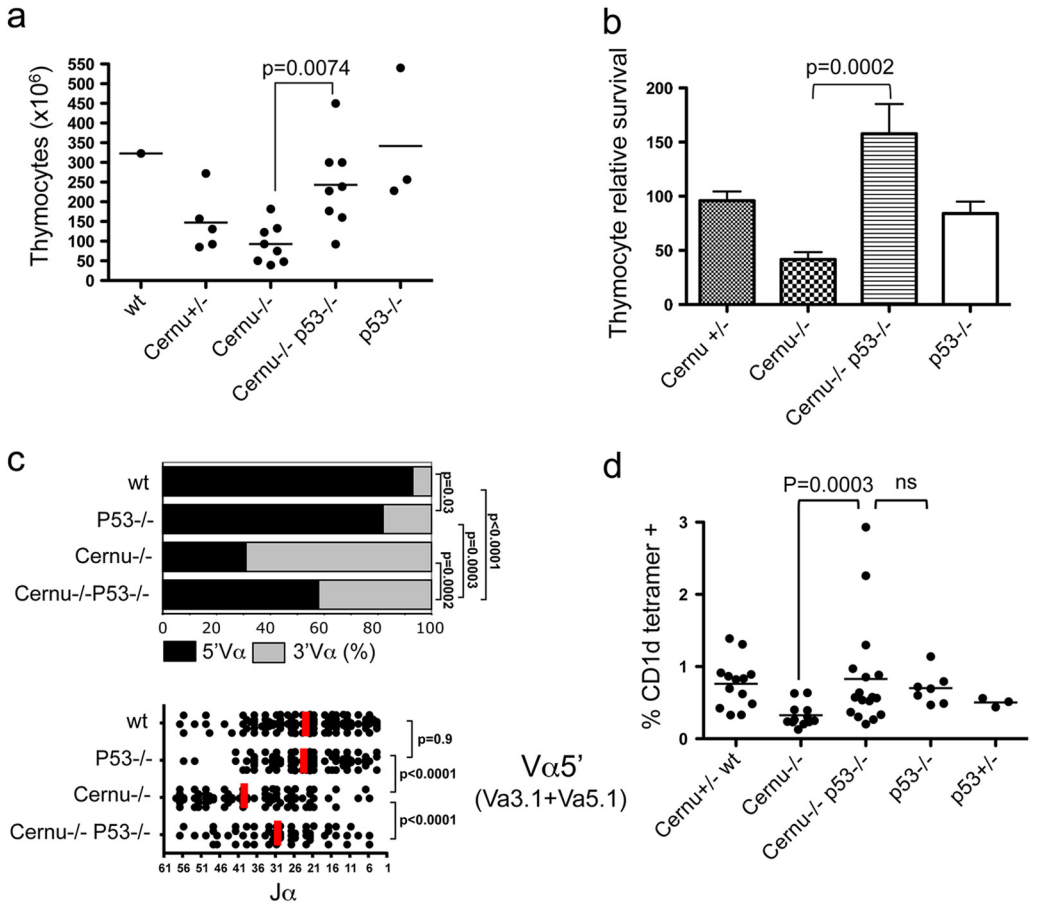

FIG 9 Partial normalization of Cernu$^{-/-}$ thymocyte viability upon P53 inactivation. (a) Total thymocyte counts. (b) Relative thymocyte survival in 24-h cultures. (c) Differential TCR Vα usage in splenic T cells, analyzed using PCR coamplification of two 5′ Vα (Va3.1 and Va5.1) and one 3′ Vα (Va3.4) segment. The vertical red lines represent the medians for Jα usage. (d) iNKT cell recovery in the spleen. ns, not significant.

ing the median of mTRAJ23 seen in wt and P53$^{-/-}$ mice (Fig. 9c). Lastly, the increased thymocyte viability in DKO mice, as revealed by TCR Vα and Jα usage, translated into a partial recovery of the iNKT cell population in DKO spleens (Fig. 9d).

We concluded that Cernunnos deficiency results in chronic activation of the DNA damage response (DDR) and subsequent P53-driven upregulation of proapoptotic factors, leading to decreased thymocyte viability and a qualitative alteration of the T cell repertoire in both humans and mice.

DISCUSSION

Cernunnos loss of function is not embryonically lethal in mice. Likewise, we identified a human Cernunnos patient harboring a homozygous genomic deletion spanning exons 2 to 5, resulting in a null allele (unpublished observation). Cernunnos is therefore not essential in both humans and mice, in contrast to Xrcc4 and DNA ligase IV.

Surprisingly, the immune system is not overwhelmingly affected in Cernu$^{-/-}$ mice, in contrast to the human Cernunnos deficiency condition (3). Indeed, while Cernunnos patients harbor a remarkable lymphopenia, the numbers of T and B lymphocytes are only slightly reduced in Cernu$^{-/-}$ mice compared to their heterozygous or wt littermates. Indeed, Cernunnos is largely dispensable during V(D)J recombination, as first noted by Li et al. (13). Accordingly, Cernu$^{-/-}$ mice crossed onto the P53 KO background did not develop B cell lymphoma, as opposed to the case with other NHEJ deficiency situations (26). We propose a speculative yet plausible explanation for this intriguing observation, based on our recent report on the Cernunnos-Xrcc4 complex structure (27). Crystals of Cernunnos-Xrcc4 complexes revealed that both homodimers associate with each other in long filaments through their head domains, helping to tether the broken DNA ends by creating a "DNA ligation synapse" (27–30). The absence of Cernunnos would then result in DNA ligation synapse destabilization rather than a catalytic malfunction of the Xrcc4-Cernunnos-DNA ligase IV complex *per se*. During V(D)J recombination, the Rag1 and Rag2 proteins persist on DNA ends, in the so-called postcleavage complex (PCC) (see the work of Schatz and Swanson [31] for a recent review), to shepherd the Rag1/2-induced DNA breaks toward the NHEJ pathway (32). The DNA end-tethering function of Xrcc4-Cernunnos filaments would then become partially redundant to the Rag1/2 PCC, arguing for the almost normal V(D)J recombination in the absence of Cernunnos. Interestingly, V(D)J recombination is severely altered in mice carrying both ATM and Cernunnos KO alleles (33), in accord with the known role of ATM in stabilizing the PCC.

We noted a significant alteration in TCR Vα and Jα usage in both murine and human Cernunnos-deficient T cells. The TCR-α

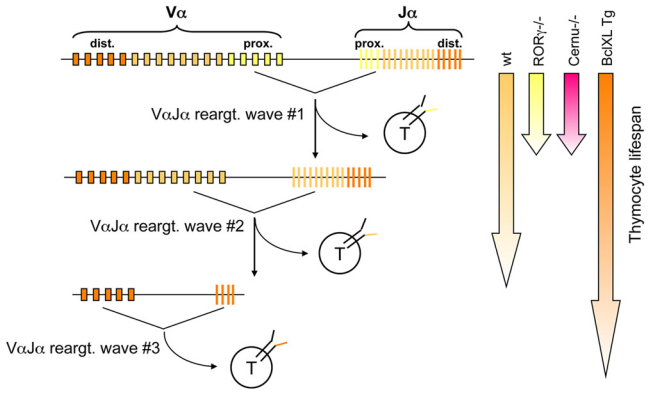

FIG 10 Multiple waves of TCR-α rearrangements during thymocyte development. DNA accessibility in the TCR Jα cluster is regulated such that the first VαJα rearrangements are targeted to the 5′ side of the TCR Jα cluster. If the thymocytes expressing the resulting TCR are not positively selected, Rag1 and Rag2 expression continues, and a second wave of rearrangement involving upstream Vα and downstream Jα segments occurs. In the absence of positive selection of this newly expressed TCR, a third wave of VαJα recombination occurs, and so on. The possibility of thymocytes undergoing several waves of TCR-α rearrangement depends on their life span. In RORγT$^{-/-}$ mice, thymocyte viability is decreased, resulting in a bias of Jα usage toward the most 5′ elements (first wave). In contrast, the thymocyte life span is increased in BclXL Tg mice, allowing several waves of recombination and the resulting skewing of Jα usage toward the most downstream elements.

locus is unique compared to the other TCR and Ig loci in the sense that multiple waves of TCR-α rearrangements can occur until the resulting TCR-expressing thymocytes are positively selected (see the work of Krangel et al. [34] for a review). The initial waves of TCR-α rearrangement involve the most 5′ Jα segments (35). Subsequent waves of VαJα rearrangements involve upstream Vα to downstream Jα segments (Fig. 10). Thymocyte viability directly affects the number of successive VαJα rearrangements (36, 37). The shift in TCR-α usage toward the most 3′ Vα segment and the most 5′ Jα segment in Cernunnos-deficient T cells in both humans and mice is therefore an indication of reduced thymocyte viability in these settings.

This is a consequence of a chronic P53 activation likely caused by a lasting DNA damage response. Indeed, introduction of the P53 KO background partially reverted the characteristics associated with thymocyte fragility. This is reminiscent of the situation of DNA ligase IV and Xrcc4 KO mice (38, 39), in which backcrossing onto the P53 KO background circumvents the embryonic lethality caused by the apoptosis of postmitotic neurons.

In conclusion, we found that although Cernunnos is dispensable for V(D)J recombination, its absence results in a skewing of TCR Vα and Jα usage, resulting in quantitative and qualitative alterations of the T cell repertoire. This is highlighted in particular by the deficit in iNKT and MAIT cells, two populations of lymphocytes expressing invariant TCRs composed of upstream Vα segments rearranged to downstream Jα segments and therefore relying on an extended thymocyte life span. Given the possible antimicrobial activity of these two discrete T cell populations (23, 40), their deficit could affect the immunocompetence of Cernunnos-defective hosts. Likewise, one cannot exclude that some other, as yet undefined T cell populations bearing particular TCR specificities could be compromised (or overrepresented) in the absence of Cernunnos. Analysis of TCR-α rearrangement in peripheral mature T cells as an indirect means to evaluate thymocyte viability could help to increase our understanding of some immune deregulation situations leading to autoimmunity or susceptibility to developing cancer.

ACKNOWLEDGMENTS

We thank P. Ferrier and M. Krangel for critical readings of the manuscript, Kamel Abdoun for animal care and anti-CD3 injections, and Christelle Lenoir for assistance in iNKT cell determination in humans. We thank the Institut Clinique de la Souris (Illkirch, France) for development of the Cernu KO mouse, the NIH Tetramer Facility for CD1d tetramers, and O. Lantz for the anti-hVα7.2 antibody.

This work was supported by institutional grants from INSERM, ERC (249816 PIDIMMUN), the Ligue Nationale contre le Cancer (Equipe Labelisée La Ligue), and GIS-Maladies Rares. G.V. was supported by the Ministère de la Recherche et de la Technologie (MRT), P.R.-M. was supported by the Institut National du Cancer and the Association de Recherche sur le Cancer (ARC), and L.M. was supported by MRT and ARC. P.R. and S.L. are scientists from CNRS.

REFERENCES

1. **Helmink BA, Sleckman BP.** 2012. The response to and repair of RAG-mediated DNA double-strand breaks. Annu. Rev. Immunol. **30**:175–202.
2. **Lieber MR.** 2010. The mechanism of double-strand DNA break repair by the nonhomologous DNA end-joining pathway. Annu. Rev. Biochem. **79**:181–211.
3. **Buck D, Malivert L, de Chasseval R, Barraud A, Fondaneche MC, Sanal O, Plebani A, Stephan JL, Hufnagel M, le Deist F, Fischer A, Durandy A, de Villartay JP, Revy P.** 2006. Cernunnos, a novel nonhomologous end-joining factor, is mutated in human immunodeficiency with microcephaly. Cell **124**:287–299.
4. **Ahnesorg P, Smith P, Jackson SP.** 2006. XLF interacts with the XRCC4-DNA ligase IV complex to promote DNA nonhomologous end-joining. Cell **124**:301–313.
5. **Andres SN, Modesti M, Tsai CJ, Chu G, Junop MS.** 2007. Crystal structure of human XLF: a twist in nonhomologous DNA end-joining. Mol. Cell **28**:1093–1101.
6. **Li Y, Chirgadze DY, Bolanos-Garcia VM, Sibanda BL, Davies OR, Ahnesorg P, Jackson SP, Blundell TL.** 2008. Crystal structure of human XLF/Cernunnos reveals unexpected differences from XRCC4 with implications for NHEJ. EMBO J. **27**:290–300.
7. **Callebaut I, Malivert L, Fischer A, Mornon JP, Revy P, de Villartay JP.** 2006. Cernunnos interacts with the XRCC4 × DNA-ligase IV complex and is homologous to the yeast nonhomologous end-joining factor Nej1. J. Biol. Chem. **281**:13857–13860.
8. **Lu H, Pannicke U, Schwarz K, Lieber MR.** 2007. Length-dependent binding of human XLF to DNA and stimulation of XRCC4.DNA ligase IV activity. J. Biol. Chem. **282**:11155–11162.
9. **Riballo E, Woodbine L, Stiff T, Walker SA, Goodarzi AA, Jeggo PA.** 2009. XLF-Cernunnos promotes DNA ligase IV-XRCC4 re-adenylation following ligation. Nucleic Acids Res. **37**:482–492.
10. **de Villartay JP.** 2009. V(D)J recombination deficiencies. Adv. Exp. Med. Biol. **650**:46–58.
11. **Brack C, Hirama M, Lenhard-Schuller R, Tonegawa S.** 1978. A complete immunoglobulin gene is created by somatic recombination. Cell **15**:1–14.
12. **Vajdic CM, Mao L, van Leeuwen MT, Kirkpatrick P, Grulich AE, Riminton S.** 2010. Are antibody deficiency disorders associated with a narrower range of cancers than other forms of immunodeficiency? Blood **116**:1228–1234.
13. **Li G, Alt FW, Cheng HL, Brush JW, Goff PH, Murphy MM, Franco S, Zhang Y, Zha S.** 2008. Lymphocyte-specific compensation for XLF/Cernunnos end-joining functions in V(D)J recombination. Mol. Cell **31**:631–640.
14. **Soulas-Sprauel P, Le Guyader G, Rivera-Munoz P, Abramowski V, Olivier-Martin C, Goujet-Zalc C, Charneau P, de Villartay JP.** 2007. Role for DNA repair factor XRCC4 in immunoglobulin class switch recombination. J. Exp. Med. **204**:1717–1727.
15. **Pasquier B, Yin L, Fondaneche MC, Relouzat F, Bloch-Queyrat C, Lambert N, Fischer A, de Saint-Basile G, Latour S.** 2005. Defective NKT cell development in mice and humans lacking the adapter SAP, the X-

linked lymphoproliferative syndrome gene product. J. Exp. Med. **201**: 695–701.
16. **Martin E, Treiner E, Duban L, Guerri L, Laude H, Toly C, Premel V, Devys A, Moura IC, Tilloy F, Cherif S, Vera G, Latour S, Soudais C, Lantz O.** 2009. Stepwise development of MAIT cells in mouse and human. PLoS Biol. **7**:e54. doi:10.1371/journal.pbio.1000054.
17. **Liang HE, Hsu LY, Cado D, Cowell LG, Kelsoe G, Schlissel MS.** 2002. The "dispensable" portion of RAG2 is necessary for efficient V-to-DJ rearrangement during B and T cell development. Immunity **17**:639–651.
18. **Villey I, Quartier P, Selz F, de Villartay JP.** 1997. Germ-line transcription and methylation status of the TCR-J alpha locus in its accessible configuration. Eur. J. Immunol. **27**:1619–1625.
19. **Pannetier C, Cochet M, Darche S, Casrouge A, Zoller M, Kourilsky P.** 1993. The sizes of the CDR3 hypervariable regions of the murine T-cell receptor beta chains vary as a function of the recombined germ-line segments. Proc. Natl. Acad. Sci. U. S. A. **90**:4319–4323.
20. **Brochet X, Lefranc MP, Giudicelli V.** 2008. IMGT/V-QUEST: the highly customized and integrated system for IG and TR standardized V-J and V-D-J sequence analysis. Nucleic Acids Res. **36**:W503–W508.
21. **van der Burg M, Gennery AR.** 2011. Educational paper. The expanding clinical and immunological spectrum of severe combined immunodeficiency. Eur. J. Pediatr. **170**:561–571.
22. **Mauvieux L, Villey I, de Villartay JP.** 2001. T early alpha (TEA) regulates initial TCRVAJA rearrangements and leads to TCRJA coincidence. Eur. J. Immunol. **31**:2080–2086.
23. **Bendelac A, Savage PB, Teyton L.** 2007. The biology of NKT cells. Annu. Rev. Immunol. **25**:297–336.
24. **Le Bourhis L, Guerri L, Dusseaux M, Martin E, Soudais C, Lantz O.** 2011. Mucosal-associated invariant T cells: unconventional development and function. Trends Immunol. **32**:212–218.
25. **Kjer-Nielsen L, Patel O, Corbett AJ, Le Nours J, Meehan B, Liu L, Bhati M, Chen Z, Kostenko L, Reantragoon R, Williamson NA, Purcell AW, Dudek NL, McConville MJ, O'Hair RA, Khairallah GN, Godfrey DI, Fairlie DP, Rossjohn J, McCluskey J.** 2012. MR1 presents microbial vitamin B metabolites to MAIT cells. Nature **491**:717–723.
26. **Ferguson DO, Alt FW.** 2001. DNA double strand break repair and chromosomal translocation: lessons from animal models. Oncogene **20**:5572–5579.
27. **Ropars V, Drevet P, Legrand P, Baconnais S, Amram J, Faure G, Marquez JA, Pietrement O, Guerois R, Callebaut I, Le Cam E, Revy P, de Villartay JP, Charbonnier JB.** 2011. Structural characterization of filaments formed by human Xrcc4-Cernunnos/XLF complex involved in nonhomologous DNA end-joining. Proc. Natl. Acad. Sci. U. S. A. **108**: 12663–12668.
28. **Andres SN, Vergnes A, Ristic D, Wyman C, Modesti M, Junop M.** 2012. A human XRCC4-XLF complex bridges DNA. Nucleic Acids Res. **40**: 1868–1878.
29. **Hammel M, Rey M, Yu Y, Mani RS, Classen S, Liu M, Pique ME, Fang S, Mahaney BL, Weinfeld M, Schriemer DC, Lees-Miller SP, Tainer JA.** 2011. XRCC4 protein interactions with XRCC4-like factor (XLF) create an extended grooved scaffold for DNA ligation and double strand break repair. J. Biol. Chem. **286**:32638–32650.
30. **Wu Q, Ochi T, Matak-Vinkovic D, Robinson CV, Chirgadze DY, Blundell TL.** 2011. Non-homologous end-joining partners in a helical dance: structural studies of XLF-XRCC4 interactions. Biochem. Soc. Trans. **39**:1387–1392.
31. **Schatz DG, Swanson PC.** 2011. V(D)J recombination: mechanisms of initiation. Annu. Rev. Genet. **45**:167–202.
32. **Lee GS, Neiditch MB, Salus SS, Roth DB.** 2004. RAG proteins shepherd double-strand breaks to a specific pathway, suppressing error-prone repair, but RAG nicking initiates homologous recombination. Cell **117**:171–184.
33. **Zha S, Guo C, Boboila C, Oksenych V, Cheng HL, Zhang Y, Wesemann DR, Yuen G, Patel H, Goff PH, Dubois RL, Alt FW.** 2011. ATM damage response and XLF repair factor are functionally redundant in joining DNA breaks. Nature **469**:250–254.
34. **Krangel MS, Carabana J, Abbarategui I, Schlimgen R, Hawwari A.** 2004. Enforcing order within a complex locus: current perspectives on the control of V(D)J recombination at the murine T-cell receptor alpha/delta locus. Immunol. Rev. **200**:224–232.
35. **Villey I, Caillol D, Selz F, Ferrier P, de Villartay JP.** 1996. Defect in rearrangement of the most 5′ TCR-J alpha following targeted deletion of T early alpha (TEA): implications for TCR alpha locus accessibility. Immunity **5**:331–342.
36. **Guo J, Hawwari A, Li H, Sun Z, Mahanta SK, Littman DR, Krangel MS, He YW.** 2002. Regulation of the TCRalpha repertoire by the survival window of CD4(+)CD8(+) thymocytes. Nat. Immunol. **3**:469–476.
37. **Sun Z, Unutmaz D, Zou YR, Sunshine MJ, Pierani A, Brenner-Morton S, Mebius RE, Littman DR.** 2000. Requirement for RORgamma in thymocyte survival and lymphoid organ development. Science **288**:2369–2373.
38. **Frank KM, Sharpless NE, Gao Y, Sekiguchi JM, Ferguson DO, Zhu C, Manis JP, Horner J, DePinho RA, Alt FW.** 2000. DNA ligase IV deficiency in mice leads to defective neurogenesis and embryonic lethality via the p53 pathway. Mol. Cell **5**:993–1002.
39. **Gao Y, Ferguson DO, Xie W, Manis JP, Sekiguchi J, Frank KM, Chaudhuri J, Horner J, DePinho RA, Alt FW.** 2000. Interplay of p53 and DNA-repair protein XRCC4 in tumorigenesis, genomic stability and development. Nature **404**:897–900.
40. **Le Bourhis L, Martin E, Peguillet I, Guihot A, Froux N, Core M, Levy E, Dusseaux M, Meyssonnier V, Premel V, Ngo C, Riteau B, Duban L, Robert D, Huang S, Rottman M, Soudais C, Lantz O.** 2010. Antimicrobial activity of mucosal-associated invariant T cells. Nat. Immunol. **11**: 701–708.